

THERMAL DECOMPOSITION OF METAL *N,N*-DIALKYL CARBAMATES: A TG-FTIR STUDY

Celia Duce^a, *Alessio Spepi*^a, *Guido Pampaloni*^{a*}, *Fabio Piccinelli*^b, *Maria Rosaria Tiné*^a

^a University of Pisa, Department of Chemistry and Industrial Chemistry, Via Moruzzi 13, 56124 Pisa, Italy.

^b University of Verona, Solid State Chemistry Laboratory-DB, Strada le Grazie 15, 37134, Verona, Italy

Abstract

Thermogravimetric analysis coupled with IR spectroscopy was used to investigate the thermal stability and decomposition products of *N,N*-dialkylcarbamates of zirconium(IV), hafnium(IV) and niobium(IV), $M(O_2CNR_2)_4$. The niobium derivatives were less stable than the corresponding Zr(IV) and Hf(IV) derivatives, and the thermal stability was in the order of $R = Et > iPr > Me$. XRD analysis of the residue showed the formation of the oxides ZrO_2 (tetragonal, $P4_2/nmc$), HfO_2 , (monoclinic, $P2_1/c$) and Nb_2O_5 (orthorhombic, $Pbam$). TEM analysis showed that all the oxides were obtained as nanopowders with a crystal size below 30 nm.

Keywords: Thermogravimetric analysis, IR spectroscopy, metal *N,N*-dialkylcarbamates, thermal stability, nanopowders

Introduction

N,N-dialkylcarbamates are a relatively recent class of compounds, containing the $[O_2CNR_2]^-$ ligand **1** (Fig. 1). This ligand is uninegative and substantially planar, due to extensive charge delocalization. The preparative aspects of compounds containing **1** has been extensively reviewed [1]. Most of the metal *N,N*-dialkylcarbamates are thermally robust compounds but in some cases, as with carbamates from high-valent transition metal cations, a reduction in the metal is observed with moderate heating depending on the nature of the R group on nitrogen [2].

*Author for correspondence: guido.pampaloni@unipi.it. Tel: +39 050 2219219
Webpage: <https://www.dcci.unipi.it/guido-pampaloni.html>

Figure 1 about here

Thermal reactions have been observed with trimethylsilyl-carbamates or mixed alkoxoalkylsilyl carbamates with the formation of isocyanates or aminosilanes/unsaturated hydrocarbons depending on the steric bulkiness of the alkyl groups [3]. In a series of papers published between 1960 and 1970, Bernard and coworkers described the thermal behaviour of alkali, alkaline earth metal and silver carbamates [4, 5]. Using DTA and TG techniques, they observed that alkali or alkaline earth metal carbamates of general formula $M(O_2CNH_2)_n$ decompose through a loss of ammonia at low temperatures. Increasing the temperature leads first to the formation of metal carbonate and then to its decomposition. For calcium, $CaCN_2$ is observed at $T > 500^\circ C$ [4]. In the case of silver, the decomposition occurs in two steps: an endothermic step at about $70^\circ C$ leading to the formation of silver imidocarbonate $NH=C(OAg)_2$, ammonia and carbon dioxide; and a second step occurring at about $120^\circ C$ forming metallic silver, ammonia, carbon dioxide and nitrogen [5].

$Zn_xMg_{x-1}O$ thin films [6] and nanosized magnetic Zn/Co oxides can be prepared by the thermal treatment of mixed Zn/Mg and Zn/Co carbamates, respectively [7]. Silver nanopowders have been obtained from silver 2-ethylhexylcarbamate at $85^\circ C$ [8].

In a previous paper [9], we reported the reaction of $Ti(O_2CNEt_2)_4$ with iron oxide nanoparticles and a TG-FTIR study of the products, including the initial titanium *N,N*-diethylcarbamate. The results thus led to the investigation of compounds of general formula $M(O_2CNR_2)_4$, $M = Zr, Hf, Nb$, $R = Me, Et, ^iPr$. Thermogravimetry, coupled with FTIR analysis of the evolved gas, is a powerful technique to investigate the thermal degradation of compounds [10]. In the present paper TG-FTIR was used to investigate the thermal stability and thermal degradation of $M(O_2CNR_2)_4$. A detailed study of the decomposition products, including XRD and TEM analysis of the residues, is also reported.

Experimental

Materials

All manipulations of air and/or moisture sensitive compounds were performed under an atmosphere of pre-purified nitrogen using standard Schlenk techniques. The reaction vessels were oven dried at $150^\circ C$ prior to use, evacuated (10^{-2} mmHg) and then filled with argon. Toluene and heptane were distilled before use from appropriate drying agents under argon atmosphere. Metal *N,N*-

dialkylcarbamates $\text{Zr}(\text{O}_2\text{CNR}_2)_4$, R = Me [11] Et [12], ⁱPr [13], $\text{Hf}(\text{O}_2\text{CNR}_2)_4$, R = Et [12], ⁱPr [12], and $\text{Nb}(\text{O}_2\text{CNR}_2)_4$, R = Me [2], Et [13], were obtained according to procedures in the literature. The crystalline samples used for the analysis were obtained by re-crystallization from hot heptane.

Methods

Powder X-ray-diffraction (PXRD) patterns were measured with a Thermo ARL X'TRA powder diffractometer, operating in the Bragg-Brentano geometry and equipped with a Cu-anode X-ray source (K_α , $\lambda = 1.5418 \text{ \AA}$), using a Peltier Si(Li) cooled solid state detector. The patterns were collected with a scan rate of 0.02 °/s in the 5°- 90° 2θ range. The phases were identified with the PDF-4+ 2013 database provided by the International Centre for Diffraction Data (ICDD). Polycrystalline samples were ground in a mortar and then placed in a low-background sample holder for data collection.

The size and morphology of the nanopowders were examined by transmission electron microscopy (TEM). The powders were suspended in 2 ml of isopropanol and a few drops of the suspensions were deposited onto copper grids and the solvent was left to evaporate at room temperature. Images were acquired using a CM12 Philips transmission electron microscope equipped with microanalysis Edax and LaB6 cathode.

A TA Instruments thermobalance model Q5000IR equipped with an FT-IR Agilent Technologies spectrophotometer model Cary 640 for Evolved Gas Analysis (EGA) was employed. TG measurements were performed at a rate of 10 °C/min, from 40 °C to 600 °C under a stream of nitrogen or air (25 ml/min). The amount of sample in each TG measurement varied between 2 and 4 mg. Each experiment was performed three times. TG-FTIR measurements were performed at a rate of 20 °C/min, from 40 °C to 500 °C under nitrogen flow (90 ml/min), from 600 to 4000 cm^{-1} with a resolution of 4 cm^{-1} . To reduce the strong background absorption from water and carbon dioxide in the atmosphere, the optical bench was purged with nitrogen. In addition, a background spectrum was taken before each analysis in order to zero the signal in the gas cell and to eliminate the contribution due to the amount of ambient water and carbon dioxide. The amount of sample in each TG-FTIR measurement varied between 6 and 8 mg. Data were collected using Agilent Resolution Pro version 5.2.0.

Results and discussion

The TG curves of the decomposition of a selection of metal *N,N*-dialkylcarbamates $M(O_2CNR_2)_4$ under nitrogen flow are presented in Figures 2, 4 and 6. The thermal decomposition of all the examined compounds shows the same degradation path both in nitrogen and in air (Figure S1 collects TG curves in air). Tables 1 and 2 summarize the TG results and the IR characterization of the volatiles evolved during the thermal treatment under nitrogen flow.

Table 1 Temperatures (maximum of DTG curve), mass loss percentage of the thermal degradation steps, and residual masses at 600°C in the decomposition of $M(O_2CNR_2)_4$ - $M = Zr, Hf, Nb$, $R = Me, Et, ^iPr$ -under nitrogen flow.

Step ^a	$Zr(O_2CNR_2)_4$			$Hf(O_2CNR_2)_4$		$Nb(O_2CNR_2)_4$		Step ^b
	R = Me	R = Et	R = ⁱ Pr	R = Et	R = ⁱ Pr	R = Me	R = Et	
1	125°C (10.6%)	80-108°C (7.8%)	72°C (1.6%)	87°C (4%)	-	54°C (14.7%)	63°C (10.9%)	1
							100-150°C (13.0%)	2
2	233°C (28.5%)	284°C (42.9%)	234°C (86.4%)	244°C (53.3%)	236°C (97.3%)	201°C (50.9%) ^c	223°C (29.0%)	3
3	290-400°C (21.9%)	300-400°C (29.7%)	351°C (8.0%)	300-400°C (20.9%)	285°C (1.3%)	250-300°C (50.9%) ^c	337°C (17.9%)	4
Residual mass at 600°C	39%	19.6%	4.0%	21.8%	1.4%	34.4%	29.2%	Residual mass at 600°C

^a Step degradation of all compounds except $Nb(O_2CNEt_2)_4$

^b Step degradation of $Nb(O_2CNEt_2)_4$

^c Total mass loss in the range 200-300°C

Table 2 Characteristic IR absorptions and temperature range of the formation of the volatiles evolved by the samples during degradation under nitrogen flow

Gas evolved	IR absorptions (cm ⁻¹) [Ref]	Temperature range (°C) of volatiles formation						
		Zr(O ₂ CNR ₂) ₄			Hf(O ₂ CNR ₂) ₄		Nb(O ₂ CNR ₂) ₄	
		R = Me	R = Et	R = ⁱ Pr	R = Et	R = ⁱ Pr	R = Me	R = Et
CO ₂	δ _{C=O} 668 ν _{C=O} 2320 and 2358 [a]	125-600	80-600	72-600	87-600	236-600	54-600	63-600
Amine	ν _{C-N} 1160, 1240-60 ν _{C-H} 2888, 2943 δ _{C-H} 1357, 1388, 1450 [b]	233-600	284-600	234-600	244-600	236-600	54-600	63-600
CO	ν _{C=O} 2104, 2180 [a]						201-600	
Tetraalkylurea	ν _{C=O} 1672 ν _{C-N} 1130-1140, 1260 ν _{C-H} 2890-2970 δ _{C-H} 1320, 1380, 1450 [b]		284-600		244-600			223-600
<i>N,N</i> -dialkyl-formamide	ν _{C=O} 1688 ν _{C-N} 1130-1140, 1260 ν _{C-H} 2810-2960 δ _{C-H} 1360, 1490 [b]	233-600					201-600	
CH ₄	ν _{C-H} 3005 [a]	233-600						

^a NIST chemistry webbook standard reference database No. 69, June 2005, release (<http://webbook.nist.gov/chemistry>).

^b Silverstein RM, Webster FX and Kiemle DJ. Spectrometric Identification of Organic Compounds, 7th Ed., Wiley, New York, 2005.

Thermal decomposition of M(O₂CNMe₂)₄, M = Zr, Nb. The thermal decomposition of M(O₂CNMe₂)₄ starts at 54°C, for niobium and at 125°C for the zirconium derivative (Fig. 2). Evolution of CO₂ and of CO₂/dimethylamine, occur in the case of the Zr and Nb, respectively (Figures S2 and S3, and Table 2). The lower thermal stability of the niobium derivative is in agreement with the instability of niobium carbamates with respect to homologous Group 4 metal derivatives [2].

Figure 2 about here

The main decomposition step of Zr(O₂CNMe₂)₄ occurs at 233°C and continues up to ca. 400°C. It is characterized by the evolution of methane, ascribable to β-elimination reactions within the NMe₂ group [14-16], and of CO₂, dimethylamine and *N,N*-dimethylformamide, as a consequence of the

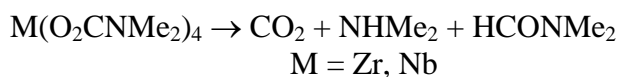
degradation of carbamate. (Fig. 3 and Table 2). The formation of *N,N*-dialkylformamides during the thermal treatment of metal carbamates can occur via deoxygenation of a carbamate unit promoted by the presence of oxophilic metals. It should be noted that the deoxygenation of CO₂ over a zinc surface has been considered responsible for the formation of *N,N*-diethylformamide and Zn₄(μ₄-O)(O₂CNEt₂)₆ during the thermal treatment of Zn with CO₂/NHEt₂ [17].

Figure 3 about here

Nb(O₂CNMe₂)₄ shows the main degradation step at 201 °C which continues up to 300°C corresponding to a total mass loss of 50.9 %, (Fig. 2). The FTIR spectrum of volatiles evolved between 200 and 300°C (Fig. S3 and Table 2) shows the formation of CO₂, together with carbon monoxide, (formed via CO₂ deoxygenation), responsible for the absorptions at 2180 and 2104 cm⁻¹ and *N,N*-dimethylformamide. By increasing the temperature from 200 to 260 °C, the signal of *N,N*-dimethylformamide at 1688 cm⁻¹ increases with respect to signals associated with carbon monoxide and dioxide.

The thermal decomposition of the products is summarized in Scheme 1.

Scheme 1. Thermal decomposition of M(O₂CNMe₂)₄, M = Zr, Nb



Thermal decomposition of M(O₂CNEt₂)₄, M = Zr, Hf, Nb. The decomposition of M(O₂CNEt₂)₄ starts at about 100 °C, or even below, with the evolution of carbon dioxide (Figure 4, and Table 1). As already noted for Nb(O₂CNMe₂)₄, the Nb(IV) ethyl derivative, Nb(O₂CNEt₂)₄, was less stable than the corresponding Zr and Hf complexes. Diethylamine and CO₂ were observed in the gas phase at the lowest temperature for niobium (63 °C compared with 80 °C and 87 °C observed for the zirconium and hafnium derivatives), (Figures S4-S6). Carbon dioxide and diethylamine are the main components of the gas phase at 284 °C (M = Zr), 244 °C (M = Hf) and 220 °C (M = Nb), (Figures 5, S4-S6, and Table 2). An absorption at 1673 cm⁻¹ can be observed (with different intensities) in the decomposition of the three carbamates. On the basis of the TG-GCMS analysis, this absorption was attributed to tetraethylurea (peak with retention time at 22.79 min).

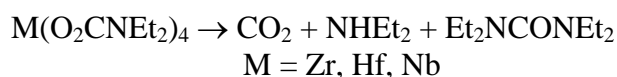
Figures 4 and 5 about here

The spectra of the volatiles obtained on heating $\text{Hf}(\text{O}_2\text{CNEt}_2)_4$ at 244°C shows an intense absorption peak at 1550 cm^{-1} (Fig. S4), which is absent in the case of the zirconium and niobium derivatives. Considering the mass loss observed during the heating procedure of $\text{Hf}(\text{O}_2\text{CNEt}_2)_4$ (Table 3), we assigned this band to the asymmetric stretching of the carbamate $-\text{CO}_2$ fragment. In fact, $\text{Hf}(\text{O}_2\text{CNEt}_2)_4$ can be sublimed (with some decomposition) at ca. 200°C / 8 mmHg. The spectral (ν_{COO} , $\text{nujol mull } 1565\text{ cm}^{-1}$) and elemental analysis (C, H, N) of the colourless sublimate confirmed the nature of the volatile product [12].

As suggested by the thermal data, the zirconium compound was less thermally stable than $\text{Hf}(\text{O}_2\text{CNEt}_2)_4$, thus only a fraction of the solid sublimed (most of it undergoes decomposition) and the 1550 cm^{-1} absorption was not observed in the gas phase spectra (Figures 5 and S4).

The thermal decomposition of the products is summarized in Scheme 2.

Scheme 2. Thermal decomposition of $\text{M}(\text{O}_2\text{CNEt}_2)_4$, $\text{M} = \text{Zr, Hf, Nb}$



Thermal decomposition of $\text{M}(\text{O}_2\text{CN}^i\text{Pr}_2)_4$, $\text{M} = \text{Zr, Hf}$. The *N,N*-diisopropylcarbamates of zirconium(IV) and hafnium(IV) $\text{M}(\text{O}_2\text{CN}^i\text{Pr}_2)_4$ showed the simplest degradation pattern. $\text{Zr}(\text{O}_2\text{CN}^i\text{Pr}_2)_4$ showed a mass loss of 1.5% at 72°C ; the main degradation step was observed at about 234°C with a mass loss of 86.4% and 97.3% for Zr and Hf samples, respectively. An additional, small mass loss was found at 351°C (8%) for Zr and 285°C (1.3%) for Hf (Fig. 6 and Table 1).

Figures 6 about here

The FTIR spectra of the volatiles evolved at 72°C for $\text{Zr}(\text{O}_2\text{CN}^i\text{Pr}_2)_4$ correspond to the emission of small quantities of carbon dioxide (Fig. S7). The same mass loss is absent in the thermal diagram of the hafnium derivative (Fig. 6), in agreement with the higher stability of derivatives of the 5d transition series with respect to the 4d series congeners [18]. None of the FTIR spectra of the volatiles evolved at 72°C by $\text{M}(\text{O}_2\text{CN}^i\text{Pr}_2)_4$ showed absorptions in the range of $1688\text{-}1673\text{ cm}^{-1}$ ascribable to *N,N*-diisopropylformamide or tetraisopropylurea.

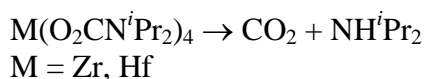
The mass loss by $\text{Zr}(\text{O}_2\text{CN}^i\text{Pr}_2)_4$ at 240°C under nitrogen flow (Fig. 7) shows signals due to CO_2 and to C–H fragments of diisopropylamine. The figure highlights an intense absorption around 1530 cm^{-1} in the spectra of the gas phases derived from the two samples. This spectrum remains substantially the same after the sample is heated at 351°C and its degradation is complete (Fig S7).

In view of the fact that the two isopropyl derivatives $M(\text{O}_2\text{CN}^i\text{Pr}_2)_4$ ($M = \text{Zr}, \text{Hf}$) can be readily sublimed (ca. 235 °C / 8 mm Hg) without (Hf) or with a reduced (Zr) decomposition, the intense absorption at around 1530 cm^{-1} was assigned to the asymmetric stretching of the carbamate- CO_2 fragment, which in the solid state occurs at 1535 (Zr) and 1540 (Hf) cm^{-1} . The ready sublimation of the two compounds is in agreement with the simple TG diagrams (Fig. 6).

Figure 7 about here

The thermal decomposition of the products is summarized in Scheme 2.

Scheme 3. Thermal decomposition of $M(\text{O}_2\text{CNEt}_2)_4$, $M = \text{Zr}, \text{Hf}, \text{Nb}$



Study of the residue at 600°C. The non-volatile, metal-containing compounds formed after the thermal treatment in nitrogen or oxygen flow of $M(\text{O}_2\text{CNR}_2)_4$, $M = \text{Zr}, \text{R} = \text{Me}; M = \text{Hf}, \text{Nb}, \text{R} = \text{Et}$, are coloured gray. The samples deriving from thermal treatments in nitrogen flow have a deeper colour than those heated in air. This suggests that the colour may be due to traces of elemental carbon (from an incomplete decomposition of the organic moiety).

X-ray powder diffraction and TEM experiments were performed in order to verify the nature of the solid residues. It was found that the residues are crystalline compounds forming well-resolved diffraction patterns, especially in the case of zirconium and niobium (see Figures S9-S11). All the residues were identified as the oxides ZrO_2 (tetragonal, $P4_2/nmc$), HfO_2 (monoclinic, $P2_1/c$) and Nb_2O_5 (orthorhombic, $Pbam$). The thermal decomposition procedure (in air or in nitrogen flow) does not lead to differences in the nature of the crystal phases. The average crystal size was estimated by the Rietveld refinement (MAUD computer program [19]) and confirmed by TEM analysis, which indicated that all the oxides powders were nanoparticles (average crystal size below 30 nm) associated in clusters of between 300 and 400 nm. (Figures 8 and S12-S13).

Figure 8 about here

Once the nature of the residues was verified, the difference between their mass (recovered at the end of the thermal treatment) and the value calculated for a stoichiometric conversion of the starting material to the metal oxides was examined. Table 3 reports the mass difference observed during the decomposition of $M(\text{O}_2\text{CNR}_2)_4$ by assuming that the residue consists of pure metal oxide.

Table 3: Mass difference (%) observed during the decomposition of $M(O_2CNR_2)_4$ by assuming that the residue consists of pure metal oxide

	M=Zr	M=Nb	M=Hf
$M(O_2CNMe_2)_4$	+ 40 %	+ 22 %	---
$M(O_2CNEt_2)_4$	- 12 %	+ 30 %	- 33 %
$M(O_2CN^iPr_2)_4$	- 78 %	-	- 95 %

As can be seen, the mass of the residues after heating $M(O_2CNMe_2)_4$, $M = Zr, Nb$, and $Nb(O_2CNEt_2)_4$ at $600^\circ C$, is higher than expected for a complete conversion to the corresponding metal oxide, thus suggesting an incomplete decomposition of the materials.

On the other hand, the mass content of the residues at $600^\circ C$ is well below the value expected for the formation of MO_2 for $Zr(O_2CN^iPr_2)_4$ and $Hf(O_2CNR_2)_4$ ($R = Et, ^iPr$). However, an almost complete sample sublimation was achieved for $Hf(O_2CN^iPr_2)_4$. Given the refractory nature of ZrO_2 and HfO_2 , the heavy mass loss proves the high volatility of the cited carbamates during the thermal decomposition.

Conclusions

The thermal analysis performed on some early transition metal *N,N*-dialkylcarbamates enabled us to draw some conclusions regarding their thermal stability and the nature of the decomposition products. In general, the $Nb(O_2CNR_2)_4$ are less stable than the corresponding $Zr(IV)$ and $Hf(IV)$ derivatives and the thermal stability is in the order of $R = Et > ^iPr > Me$; *i.e.*, *N,N*-dimethylcarbamates being the least stable of the series.

The thermal decomposition generally starts with the loss of CO_2 below $100^\circ C$ and continues with a main decomposition step in the temperature range $200-300^\circ C$ with the evolution of CO_2 and amines. When the temperature is increased, *N,N*-dimethyl- and *N,N*-diethylcarbamates produce *N,N*-disubstituted formamides or tetraalkylureas during the main decomposition step.

N,N-diisopropylcarbamates and $Hf(O_2CNEt_2)_4$ show the simplest degradation pattern due to the high volatility of these mononuclear species which readily sublime in vacuo. The formation of volatile species accounts for the low values of the residual mass obtained at $600^\circ C$.

A combination of XRD and TEM analyses of the residues showed the formation of ZrO₂, HfO₂ and Nb₂O₅. TEM analysis showed that all of the oxides were obtained as nanopowders with a crystal size below 30 nm.

Acknowledgements

The authors wish to thank Dr. Ronan Cozic and Dr. Tiffany Marre (S.R.A.Instruments France, Lyon) for the execution of TG-GCMS measurements on M(O₂CNEt₂)₄. This work was supported by the projects PRIN 2010-2011 (2010C4R8M8) and FIRB 2012 (RBF12ETL5), funded by the Italian Ministry of University and Research, and by the project PRA-2015 funded by the University of Pisa.

References

- [1] Belli Dell'Amico D, Calderazzo F, Labella L, Marchetti F and Pampaloni G. *Chem Rev.* 2003, 103:3857-3897.
- [2] Forte C, Pampaloni G, Pinzino C and Renili F. *Inorg Chim Acta* 2011; 365:251-255.
- [3] Szalay R, Böcskei Zs, Knausz D, Lovász Cs, Ujszászy K, Szakács L and Sohár P. *J Organomet Chem* 1996;510: 93-102.
- [4] Bernard MA, Borel MM and Chauvenet G. *Bull Soc Chim Fr* 1965;2122-2124.
- [5] Bernard MA and Laisne JP. *Bull Soc Chim Fr* 1970; 2938-2940.
- [6] Hill MR, Jensen P, Russell JJ and Lamb RC. *Dalton Trans* 2008;2751-2758.
- [7] Domide D, Walter O, Behrens S, Kaifer E and Himmel HJ. *Eur J Inorg Chem* 2011; 860-867.
- [8] Kim KY, Gong MS and Park CK. *Bull Korean Chem Soc* 2012; 33:3987-3992.
- [9] Dolci S, Domenici V, Duce C, Tiné MR, Ierardi V, Valbusa V, Jaglicic Z, Boni A, Gemmi M and Pampaloni G. *Mat Res Expr* 2014; 1: 035401-035420.
- [10] Duce C, Vecchio Cipriotti S, Ghezzi L, Ierardi V and Tinè MR. *J Therm Anal Calorim.* 2015, 121:1011-1019.
- [11] Chisholm MH and Extine MW. *J Am Chem Soc* 1977; 99:782-792.
- [12] Calderazzo F, Ianelli S, Pampaloni G, Pelizzi G and Sperrle M. *J. Chem. Soc., Dalton Trans* 1991;693-698.
- [13] Arimondo PB, Calderazzo F, Englert U, Maichle-Mössmer C, Pampaloni G and Strähle J. *J. Chem. Soc., Dalton Trans* 1996;311-319.

- [14] Au CC, Lai TH and Chan KS. *J Organomet Chem.* 2010; 695:1370-1374.
- [15] Bradley DC and Thomas IM. *Can J Chem* 1962; 40:449-454.
- [16] Bradley DC and Thomas IM. *Can J Chem* 1962; 40:1355-1360.
- [17] Belforte A, Calderazzo F, Englert U and Strähle J. *Inorg Chem* 1991;30:3878-3881.
- [18] Cotton FA, Wilkinson G, Murillo CA and Bochmann M. *Advanced Inorganic Chemistry*, 6th Ed. J. Wiley, New York, 1999.
- [19] Lutterotti L and Gialanella S. *Acta Mater.* 1998; 46:101-110.

Figure Captions

Fig.1 The *N,N*-dialkylcarbamato ligand.

Fig.2 TG curves (left axis) and their derivatives (right axis) of $\text{Zr}(\text{O}_2\text{CNMe}_2)_4$ and $\text{Nb}(\text{O}_2\text{CNMe}_2)_4$, obtained under nitrogen flow at $10^\circ\text{C}/\text{min}$ heating rate.

Fig.3 FTIR spectrum of the volatiles evolved under nitrogen flow by $\text{Zr}(\text{O}_2\text{CNMe}_2)_4$ at 233°C .

Fig.4 TG curves (left axis) and their derivative (right axis) of $\text{Zr}(\text{O}_2\text{CNEt}_2)_4$, $\text{Hf}(\text{O}_2\text{CNEt}_2)_4$ and $\text{Nb}(\text{O}_2\text{CNEt}_2)_4$, performed under nitrogen flow at $10^\circ\text{C}/\text{min}$ heating rate.

Fig.5 FTIR spectrum of the volatiles evolved under nitrogen flow by $\text{Zr}(\text{O}_2\text{CNEt}_2)_4$ at 284°C .

Fig.6 TG curves (left axis) and their derivatives (right axis) of $\text{Zr}(\text{O}_2\text{CN}^i\text{Pr}_2)_4$ and $\text{Hf}(\text{O}_2\text{CN}^i\text{Pr}_2)_4$, performed under nitrogen flow at $10^\circ\text{C}/\text{min}$ heating rate.

Fig.7 FTIR spectrum of the volatiles evolved under nitrogen flow by $\text{Zr}(\text{O}_2\text{CN}^i\text{Pr}_2)_4$ at 240°C .

Fig.8 TEM image of the solid residue obtained upon thermal treatment in air flow of $\text{Zr}(\text{O}_2\text{CNMe}_2)_4$ at 600°C .